Supplementary Information

Near Room-Temperature Chemical Vapor Deposition of 2D SbI_3 on Van der Waals Substrates for Photodetector Applications

Ziliang Zhao‡[a], Ming Wu‡[b], Hao Wu[a], Xiangzhou Chen[a], Haiyan Ma[a], Dehu Li[a], Guanzhong Wang[a], Qiuyun Yang[a,c]*, Zhibin Shao[b]* and Hong Wang[a]*

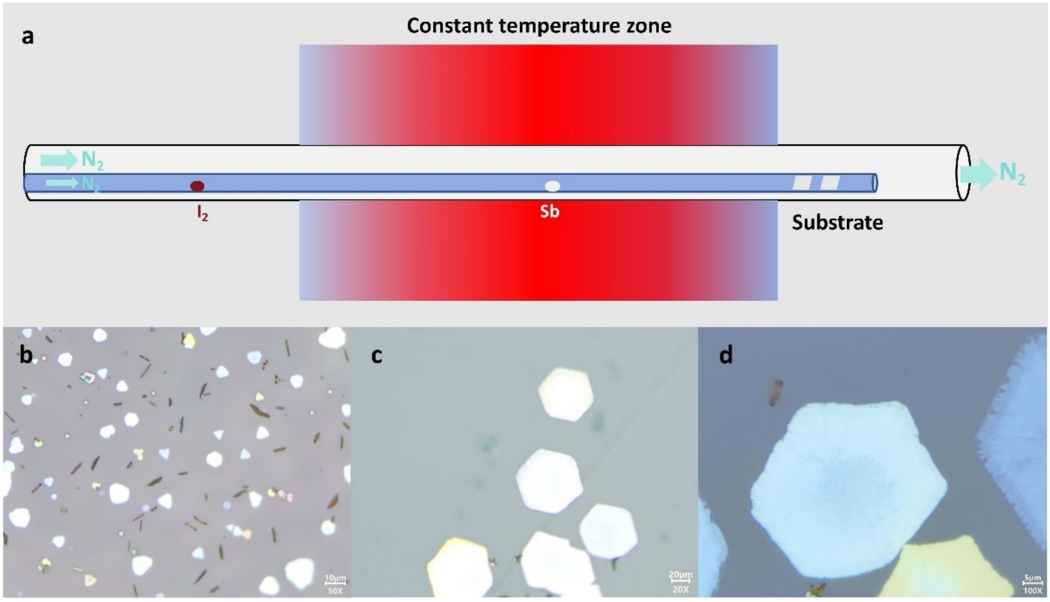

Figure S1. Antimony triiodide synthesized on mica substrates. (a) Schematic illustration of an CVD growth setup. (b–d) Optical images of SbI_3 thin crystals grown on mica substrate.

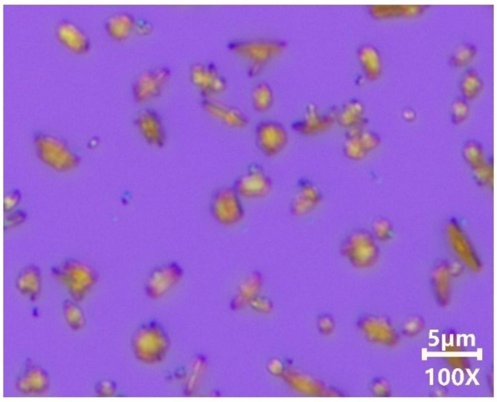

Figure S2. Optical images of SbI_3 grown on SiO_2/Si substrate.

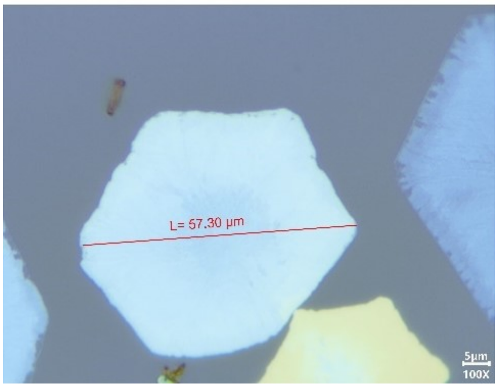

Figure S3. Optical image of the SbI_3 thin crystal. The optical image shows that the size of single crystal SbI_3 can reach up to 50 μm.

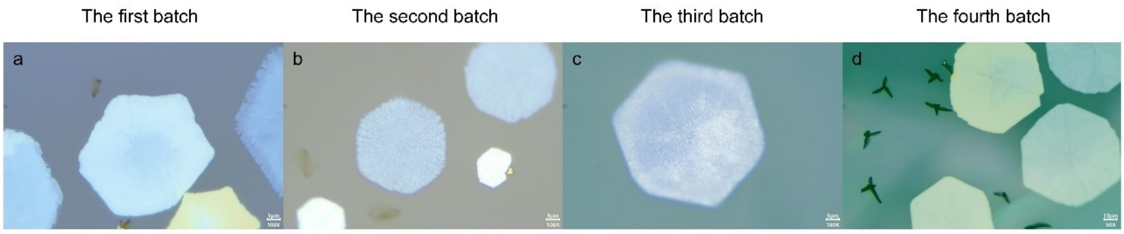

Figure S4. Optical images of SbI_3 thin crystals on mica substrates. (a) First batch of the SbI_3 samples. (b) Second batch of the SbI_3 samples. (c) Third batch of the SbI_3 samples. (d) Fourth batch of the SbI_3 samples.

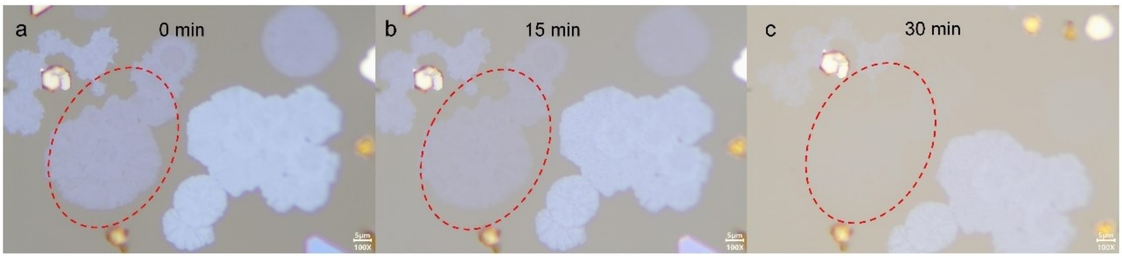

Figure S5. Air stability of the sample characterized by optical images. (a) The optical images of the as-prepared sample. (b) The optical images of the sample exposed in air for 15 min. (c) The optical images of the sample exposed in air for 30 min.

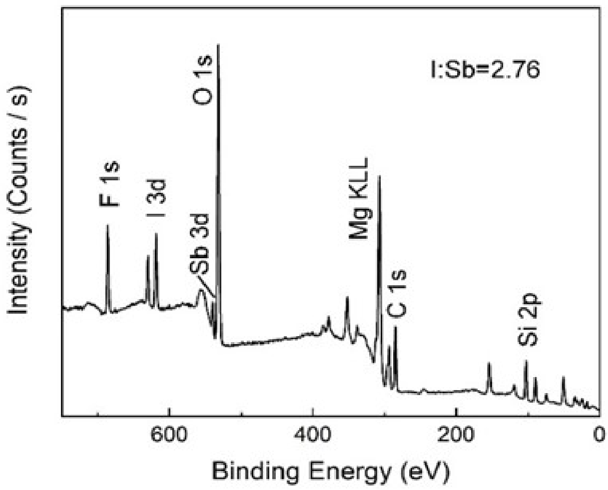

Figure S6. X-ray photoelectron spectroscopy (XPS) survey spectra of SbI_3 on mica.

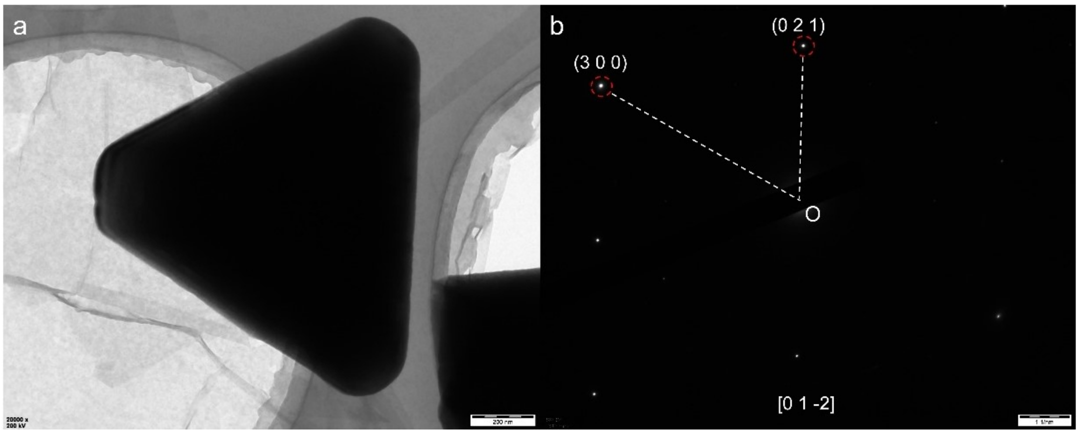

Figure S7. (a) Low-magnification TEM image of a SbI_3 crystal. (b) SAED pattern of SbI_3.

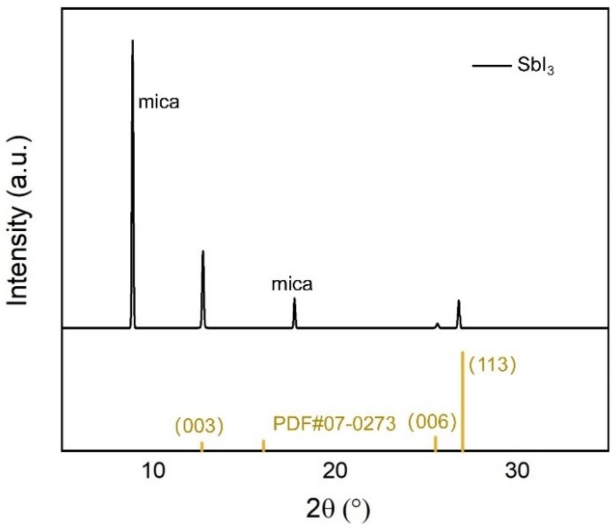

Figure S8. X-ray diffraction (XRD) pattern of SbI_3 on mica.

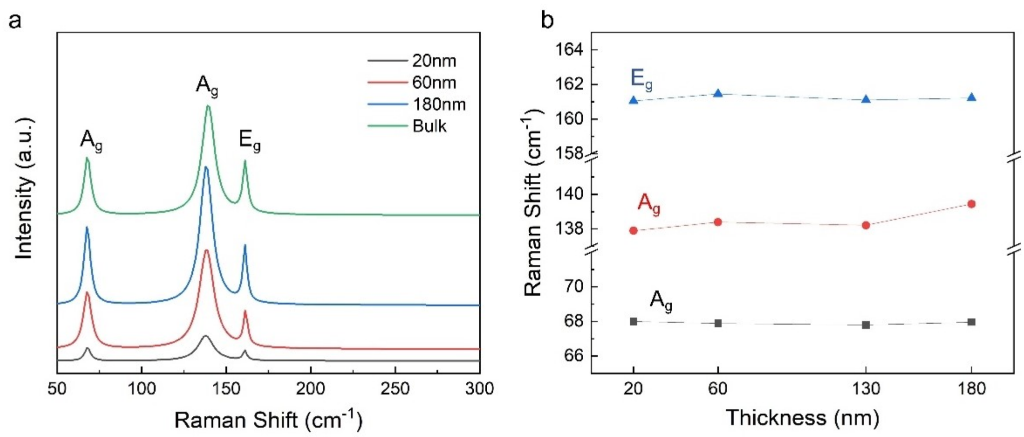

Figure S9. Raman spectroscopy of Antimony triiodide. (a) Raman spectra of SbI_3 with thicknesses varying from 20 nm to bulk. (b) A_g, E_g peak frequencies plotted against sample thickness.

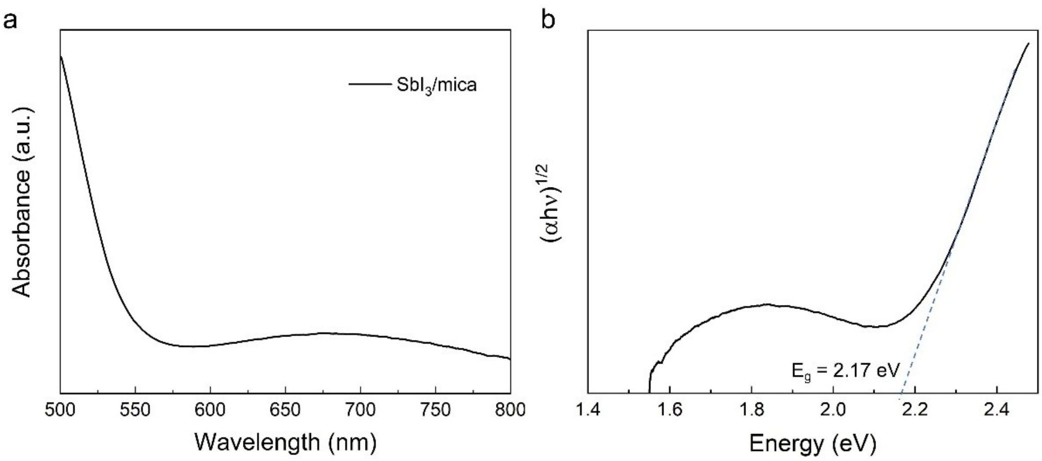

Figure S10. The optical absorption spectra of Antimony triiodide. (a) UV-vis absorption spectra of SbI_3. (b) The Tauc plot method for determining the bandgap of SbI_3.

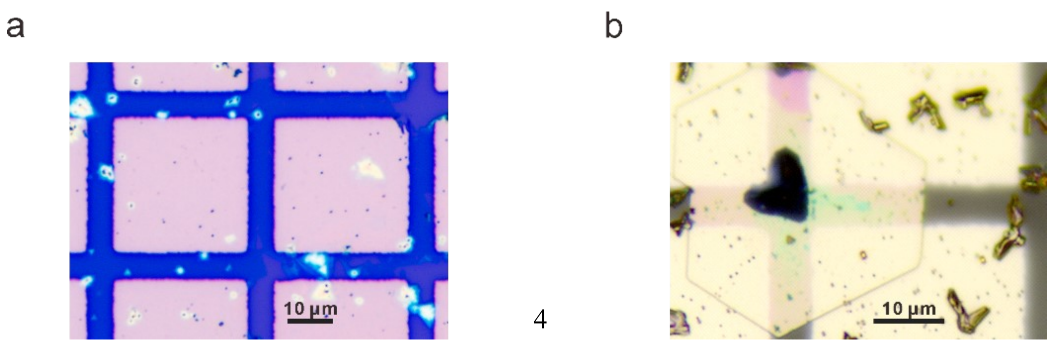

Figure S11. Optical microscopy images of (a) a WS_2 and (b) a SbI_3 devices. Notably, the WS_2 region is large and extends across the entirety of the area depicted in Figure a.

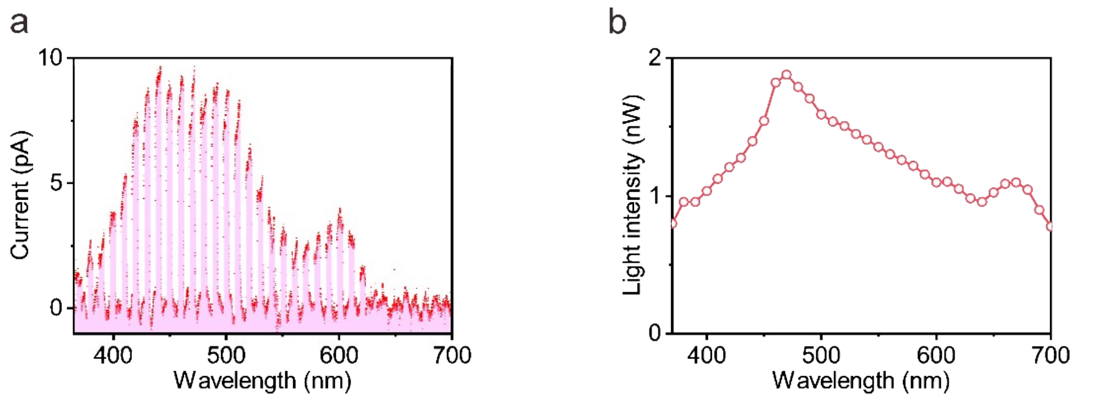

Figure S12. (a) Photoresponse curves measured at a 1 V bias under illumination with monochromatic light of progressively increasing wavelengths. (b) Intensity of monochromatic light as a function of wavelength.

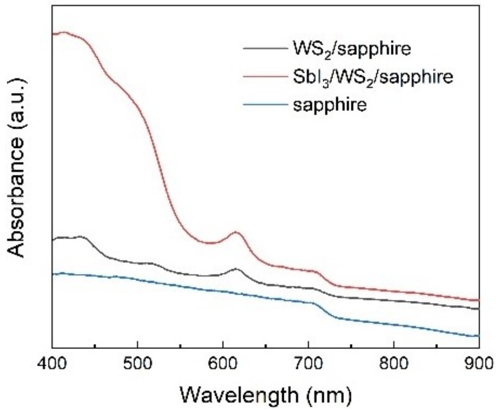

Figure S13. The optical absorption spectra of WS_2 and SbI_3/WS_2 heterostructure on sapphire substrates.

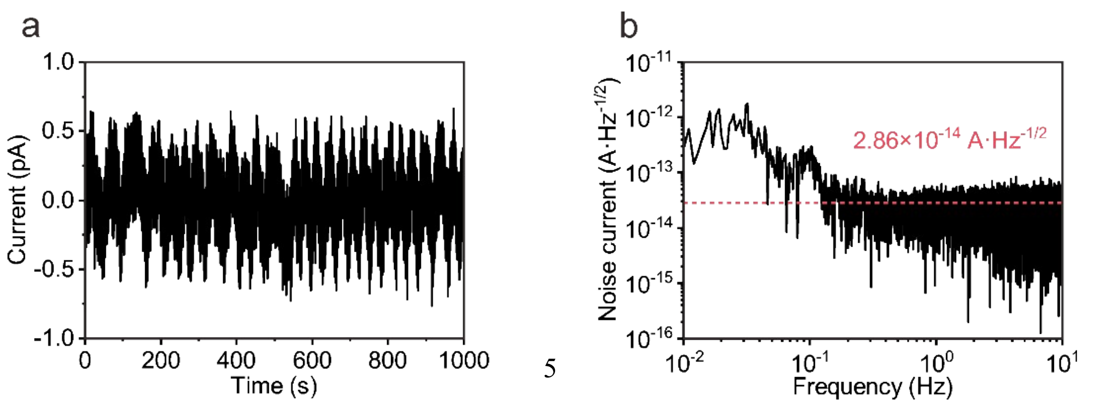

Figure S14. (a) Time-resolved dark current of a SbI_3-modified WS_2 photodetector measured under dark condition at V=1 V and (b) Noise spectral density curve derived from the Fourier transform of the dark current traces, illustrating the frequency-dependent characteristics of the noise signal.

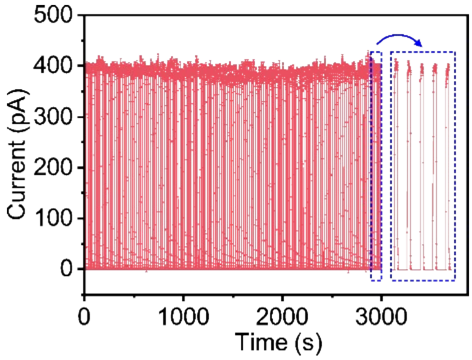

Figure S15. Photoresponse curve recorded over 3000 seconds under cyclic illumination at a wavelength of 520 nm.

Table S1. Responsivity comparison of pristine WS_2 Photodetectors and Sensitizer-Modified WS_2 Photodetectors.

Device material	**Bias voltage (V)**	**Responsivity ($A\cdot W^{-1}$)**	**Reference**
Multilayer WS_2	5	9.2×10^{-5}	[1]
Monolayer WS_2	10	5×10^{-3}	[2]
SnSe/Monolayer WS_2	5	9.9×10^{-2}	[3]
BP/WS_2	5	1.2×10^{-1}	[4]
GOQDs/WS_2	5	1.25×10^{-2}	[5]
CdSe-QDs/WS_2	10	2×10^{-5}	[6]
$PdSe_2/WS_2$	2	3.91×10^{-3}	[7]
SbI_3/WS_2	1	1.58×10^{-2}	this work

Table S2. Performance comparison for WS_2-based photodetectors incorporating advanced responsivity enhancement strategies.

Photodetectors	**Strategy**	**Bias voltage**	**Responsivity ($A\cdot W^{-1}$)**	**Reference**
Au NPs/WS_2	Plasmonic	2 V	1050	[8]
In atoms/WS_2	Photogating	V_{ds} = 1 V V_{gs} = 2 V	2630	[9]
WSe_2 puddle/WS_2	Photogating	V_{ds} = 3 V V_{gs} = 40 V	300	[10]
Si/WS_2	Heterojunction	5 V	8.3	[11]
MoS_2/WS_2	Heterojunction	-	2.3	[12]

References

1. N. Perea-López, A. L. Elías, A. Berkdemir, A. Castro-Beltran, H. R. Gutiérrez, S. Feng, R. Lv, T. Hayashi, F. López-Urías, S. Ghosh, B. Muchharla, S. Talapatra, H. Terrones and M. Terrones, *Advanced Functional Materials*, 2013, **23**, 5511-5517.
2. C. Lan, Z. Zhou, Z. Zhou, C. Li, L. Shu, L. Shen, D. Li, R. Dong, S. Yip and J. C. Ho, *Nano Research*, 2018, **11**, 3371-3384.
3. Z. Jia, J. Xiang, F. Wen, R. Yang, C. Hao and Z. Liu, *ACS Applied Materials & Interfaces*, 2016, **8**, 4781-4788.
4. Z. Jia, J. Xiang, C. Mu, F. Wen, R. Yang, C. Hao and Z. Liu, *Journal of Materials Science*, 2017, **52**, 11506-11512.
5. H. J. W. Li, K. Huang and Y. Zhang, *Materials Research Express*, 2019, **6**, 045902.
6. Q. Feng, Y. Li, F. Gao, Y. Sun, J. Yan, W. Liu, H. Xu and Y. Liu, *ACS Photonics*, 2020, **7**, 1857-1865.
7. X. Kang, C. Lan, F. Li, W. Wang, S. Yip, Y. Meng, F. Wang, Z. Lai, C. Liu and J. C. Ho, *Advanced Optical Materials*, 2021, **9**, 2001991.
8. Y. Liu, W. Huang, W. Chen, X. Wang, J. Guo, H. Tian, H. Zhang, Y. Wang, B. Yu, T.-L. Ren and J. Xu, *Applied Surface Science*, 2019, **481**, 1127-1132.
9. C.-H. Yeh, H.-C. Chen, H.-C. Lin, Y.-C. Lin, Z.-Y. Liang, M.-Y. Chou, K. Suenaga and P.-W. Chiu, *ACS Nano*, 2019, **13**, 3269-3279.
10. T.-H. Tsai, Z.-Y. Liang, Y.-C. Lin, C.-C. Wang, K.-I. Lin, K. Suenaga and P.-W. Chiu, *ACS Nano*, 2020, **14**, 4559-4566.
11. E. Wu, D. Wu, C. Jia, Y. Wang, H. Yuan, L. Zeng, T. Xu, Z. Shi, Y. Tian and X. Li, *ACS Photonics*, 2019, **6**, 565-572.
12. Y. Xue, Y. Zhang, Y. Liu, H. Liu, J. Song, J. Sophia, J. Liu, Z. Xu, Q. Xu, Z. Wang, J. Zheng, Y. Liu, S. Li and Q. Bao, *ACS Nano*, 2016, **10**, 573-580.